Journal of Materials Research and Technology 31 (2024) 1229–1235

Contents lists available at ScienceDirect

Journal of Materials Research and Technology

journal homepage: www.elsevier.com/locate/jmrt

New approach to niobia-modified borosilicate glasses for Cs waste immobilization

D.L. Costa-Silva [a], M.S. Araujo [a], D.A. Fungaro [b], P.S.C. Silva [c], S. Mello-Castanho [a,*]

[a] Centro de Ciência e Tecnologia de Materiais (CECTM), Instituto de Pesquisas Energéticas e Nucleares, IPEN/CNEN, Av. Prof. Lineu Prestes, 2242 – Cidade Universitária, CEP 05508-000, São Paulo, SP, Brazil
[b] Centro de Química e Meio Ambiente (CEQMA), Instituto de Pesquisas Energéticas e Nucleares, IPEN/CNEN, Av. Prof. Lineu Prestes, 2242 – Cidade Universitária, CEP 05508-000, São Paulo, SP, Brazil
[c] Centro do Reator de Pesquisa (CERPQ), Instituto de Pesquisas Energéticas e Nucleares, IPEN/CNEN, Av. Prof. Lineu Prestes, 2242 – Cidade Universitária, CEP 05508-000, São Paulo, SP, Brazil

ARTICLE INFO

Handling Editor: SN Monteiro

Keywords:
Sugarcane bagasse ash
Radioactive cesium
Niobium aluminoborosilicate glasses
Cs-loaded zeolite a

ABSTRACT

The use of nuclear materials is increasing in energy production, medicine, and environmental sectors. Following this trend, the generation of radioactive wastes is also increasing in the whole production cycle and use of this kind of materials. Among these, the ^{137}Cs radionuclide presents a potential risk to human health due to its half-life time (30,2 years), high-level activity (1 TBq) and easiness to contaminate rivers, soil, and air. The immobilization of ^{137}Cs in solid matrices has been an available option researched by several countries. In this context a new glass composition based on aluminoborosilicate glass modified with niobium (Nb) was used for the immobilization of cesium through adding Cs-loaded zeolite. Homogeneous vitreous wasteforms were improved with the growth of Nb content in the compositions. All compositions were able to keep up to 5.9 wt% Cs_2O, previously adsorbed by zeolite A, and the immobilization efficiency was around 53%. Their structural analyses by Raman revealed a depolymerized and complex network structure, due to the presence of several cations including Cs. In turn, Nb reflected positively on the chemical resistance and thermal properties, by changing the distribution of silicate species. The wasteforms presented good glass forming ability and thermal stability up to 520 °C. Through the thermal treatment for devitrification, Cs atoms were stabilized into the Pollucite phase ($CsAlSi_2O_6$). Besides that, the wasteforms, preferably the one containing 8.0 mol% Nb, showed low elemental releases and leaching rates for Cs (1×10^{-3} g m^2.day^{-1}), after the leaching experiments at 90 °C for 7 days in static conditions, verified by the neutron activation analysis (NAA).

1. Introduction

The worldwide increase in nuclear power production has a consequence, as massive amounts of radioactive waste are currently produced in the nuclear power plants, and such waste can seriously contaminate the environment through soil and water [1]. Fission products such as technetium (^{99}Tc) and ^{137}Cs derive from nuclear reactions and have gained a special attention after accidents occurred in nuclear power plants such as Chernobyl (Ukraine, 1986) and Fukushima (Japan, 2011) [2]. Among the cesium radionuclides (^{134}Cs, ^{135}Cs, and ^{137}Cs) commonly found in inventories [3],^{137}Cs is one of the most dangerous due to its long half-live (30.2 years), high-level activity (1 TBq) and because it can be distributed on the soil surface, threatening the ecosystem, the food chain and human health [4]. The removal of superficial layers of contaminated soil produces a great amount of high-level radioactive waste (HLW), and this procedure has been done in some areas affected by nuclear accidents, treating around 22.5 million tons of waste [5]. Therefore, the reduction and disposal of this amount of waste is extremely important.

In this context, several inorganic adsorbent materials have been used for decontamination of ^{137}Cs from liquid radioactive wastes, such as natural bentonite, ferrocyanides, melamine-styrene, synthetic and natural zeolites [2,6–9]. However, besides the high selectivity for Cs that all these materials exhibit, they are commonly used in intermediate stages of the HLW immobilization processes, due to their low retention stability in contact with water, and are fixed in matrices such as cement blends, geopolymers, and glasses [10–12].

The vitrification of HLW has been performed over decades, as a

* Corresponding author.
E-mail address: srmello@ipen.br (S. Mello-Castanho).

https://doi.org/10.1016/j.jmrt.2024.06.099
Received 4 April 2024; Received in revised form 29 May 2024; Accepted 14 June 2024
Available online 15 June 2024

method for the immobilization of around 34 radionuclides into glasses and glass-ceramics, whose composition varies depending on the chemical nature of the wastes [3]. Borosilicate glasses are the most used matrices, for exhibiting ease of processing, compositional adaptation and long-term integrity [13–15]. Waste elements can be incorporated in the glass network structure when the solubility at the melting temperature is high enough. When considering a vitreous matrix for NW immobilization, three initial principles are to be analyzed: (1) the ability to accommodate the different waste elements; (2) the vitrification process, that includes the melting temperature, reactivity, viscosity of the mixtures and (3) the glass performance regarding the mechanical, chemical, thermal and radiation resistances [16]. All these factors are important variables that impact on long-term behavior of the wasteform.

In a previous work, we have shown that up to 8.0 mol% of Nb additions can be performed in an aluminoborosilicate glass composition, causing slight disturbances in the network structure that resulted in the increase of the glass thermal and chemical stability. However, the solubility limit (8.0 mol%) was observed, with a trend towards the growth of a niobium-rich sub-network [17].

In this work, we applied the referred glass matrices in the vitrification of a fixed proportion of Cs-loaded zeolitic material. The influence of distinct Nb contents in the behavior of important properties such as the thermal stability, the structural changes and the leaching behavior of the simulated wasteforms were evaluated as a safe option to fix the water unstable Cs-loaded waste into bulk glassy materials. As a challenge, some characteristics of these nuclear glass wasteforms were evaluated, with a focused insight on the atomic structure of this glass system, in search of materials that present high thermal stability and reduced leaching rates.

2. Experimental procedure

2.1. Vitrification process

The vitrification proposed in this work is a process dealing with one of the possible treatments of ^{137}Cs-rich nuclear effluents, using the stable nuclide (^{133}Cs) as simulated nuclear waste. The vitrification starts with the synthesis of type A zeolite, whose procedure can be found in previous work [18], using sugarcane bagasse ash (SCBA) as Si source. After the synthesis, the zeolitic material was submitted to the adsorption experiment, by using an aqueous solution of CsCl (99.9%) (100:1 H_2O/CsCl mass ratio) and zeolite (100:1 H_2O/zeolite mass ratio), stirred for 24 h, filtered and dried in oven (16 h), adapted from the procedure found in the literature [19]. A fixed proportion of Cs-loaded waste was incorporated into the glasses (2:3 wt proportion), by mixing with the glass precursors (reagent-grade: SiO_2, NaOH, CaO, Al_2O_3, H_3BO_3, metallic Nb powder and K_2CO_3) and homogenization. After the mixing, the materials were transferred to alumina crucibles for melting at 1280 °C in an electrical furnace, during 1.5 h in atmospheric air, and were cast into a metallic plate for super-fast cooling and solidification. Three simulated wasteform compositions were prepared, containing increasing contents of Nb in substitution of SiO_2. The specimens are designated by V (for glasses); Z-Cs (for Cs-loaded zeolite) and the numbers 2, 4 and 8 are related to Nb contents (mol%), whose nominal composition belongs to the system (in mol%):

$$(100\text{-}x)44.2SiO_2\text{-}xNb_2O_5\text{-}25.2Na_2O\text{-}21.7CaO\text{-}7.0B_2O_3\text{-}1.2Al_2O_3\text{-}0.7K_2O.$$

2.2. Characterization techniques

X-ray diffraction measurements were conducted using Cu-Kα radiation, with 0.05°/s by step. The Raman spectra were collected from wasteforms samples in a confocal Raman microscope, using Ar^+ laser (532 nm) at room temperature. The spectra were corrected with Bose-Einstein thermal factor, the deconvolution performed with Fityk [20], and the bands assignments were based on the literature [21–23]. Chemical analyses were performed by using Energy Dispersive X-ray Fluorescence Spectrometry (ED-XRF) for all elements, except boron, whose concentration shown is related to previous results obtained by ICP-OES on these glass matrices (without zeolite incorporation) [17]. Differential thermal analyses (DTA) were conducted in the wasteforms specimens up to 1000 °C, in synthetic air, and at a 10 °C/min heating rate. The crystallization behavior of glass specimens was observed through thermal treatments (520 °C, 685 °C and 800 °C) during 2 h, in atmospheric air, and the thermal stability was evaluated by calculating the Hrubý parameter [24].

Evaluation of the chemical resistance was conducted by leaching tests according to ASTM C1285-02 (PCT-B). The glass wasteform samples were grinded (mean diameter of 320 nm), agitated in acetone and dried, using high waste surface area/leachate volume (697 m^2/L). The elemental concentration on the leachants from the PCT-B tests was determined by inductively coupled plasma - optical emission spectrometry (ICP-OES). Melt homogeneity was evaluated through transmitted light optical microscopy by using equipment with achromatic objective lens. The concentration of Cs and Nb on the PCT-B aliquots was determined by Neutron Activation Analysis (NAA), by using the IEA-R1 nuclear research reactor at IPEN (Instituto de Pesquisas Energéticas e Nucleares), by irradiation under a thermal neutron flux of $10^{12}cm^{-2}s^{-1}$ for 8 h. The counting of radionuclide (^{134}Cs) was performed after 15 days cooling by gamma spectrometry, using a highly pure Ge detector (HPGe) coupled to a DSA-1000 multichannel analyzer. The method was attested by analyzing the reference material USGS STM-2.

3. Results and discussion

The results presented here are an interesting contribution to the development of nuclear waste immobilization processes, and special attention is particularly given to ^{137}Cs due its elevated risk to human health. The immobilization of ^{137}Cs in adequate glasses is an important process towards the retention and safe immobilization of these elements in bulk materials, otherwise these radionuclides would present high volatility and mobility through water systems [19,25–27]. The benefits of Nb in some characteristics of the wasteforms such as thermal, structural, and leaching properties are discussed in this section.

The XRD pattern of the raw zeolite produced from sugarcane bagasse ash (SCBA) and the Cs-loaded zeolite sample after the adsorption experiment is shown in Fig. 1, and suggests high crystallinity for the zeolitic material obtained, which is identified as Na-A type zeolite (JCPDS 43–0142). The presence of peaks at 20.8 and 26.5° (2θ) related to quartz (SiO_2) indicates minor residues of this component, however, the synthesized zeolite is highly phase pure. In addition, the pattern of the Cs-loaded zeolite (JCPDS 86–2353) sample shows changes in intensity of several peaks, disappearance of peaks (111), (420), (421), (500), (520), (521), (441), (530), (531) and (621), also with emergence of peaks (222) and (321). All these changes are due to the exchange of Na^+ (ionic radius 1.02 Å) for Cs^+ (ionic radius 1.69 Å), causing lattice strain, as Cs^+ occupy 8-membered rings.

The chemical composition of the Cs-loaded zeolite and glass wasteforms, exhibited in Table 1, shows that, except for the planned variation of SiO_2 and Nb_2O_5, little fluctuations are observed for CaO and Na_2O, however they were kept relatively stable, and values represent 60 wt% of the glass matrices utilized, as planned. The incorporation of Cs-loaded zeolite (40 wt.% of the total mixture) into the wasteform resulted in a final Cs_2O content of up to 5.9 wt.%. This value is lower than the initially projected 11.3 wt.%, suggesting the partial volatilization of Cs from the zeolite during the melting process (1280 °C). Consequently, the overall immobilization efficiency of Cs in the wasteform was determined to be approximately 53%. Therefore, future adaptations such as the possible use of crucible caps, and addition of flux agents in the glass composition

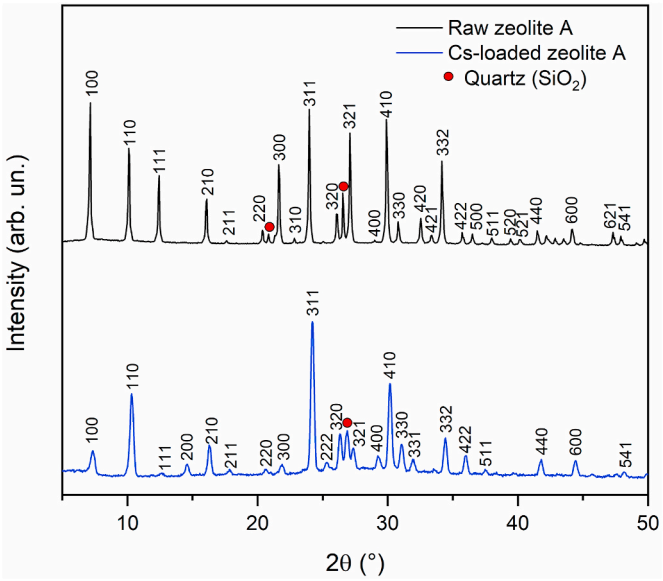

Fig. 1. XRD patterns of the raw zeolite A sample and Cs-loaded zeolite A after the adsorption experiment.

Table 1
Chemical composition (wt.%) of the glass sample wasteforms (VZ-Cs) and the Cs-loaded zeolite A, obtained by energy dispersive X-ray fluorescence (ED-XRF).

Component	V2Z-Cs	V4Z-Cs	V8Z-Cs	Cs-loaded zeolite
SiO_2	42.86	41.77	37.42	26.97
Na_2O	15.79	14.41	13.29	–
B_2O_3	4.80	4.79	4.81	–
Nb	1.83	3.63	7.98	–
Cs_2O	4.85	5.29	5.91	28.30
Al_2O_3	13.81	13.62	14.17	22.99
CaO	12.39	12.77	13.27	–
Fe_2O_3	–	–	–	7.01
L.O.I.[a]	–	–	–	14.59
Other	3.67	3.72	3.15	0.14

[a] Lost on ignition.

will be considered, to reduce the melting temperature and capture volatilized Cs, reintroducing it into the melt for loss mitigation.

The homogeneity of the wasteforms specimens, as illustrated by Fig. 2 for samples V2Z-Cs, V4Z-Cs and V8Z-Cs, revealed marked differences in the macrostructure after melting at the same preparing conditions. A different scenario can be observed for V2Z-Cs and V4Z-Cs when compared to V8Z-Cs, which exhibits a "liquid-like" aspect predominantly homogenous, and these results also confirm the influence in macro levels of the Nb contents on the melting response.

In our previous work we have shown that distinct Nb contents (up to 8.0 mol%) in the base compositions of these glass matrices cause some disturbance in the network structure resulting in the reduction of the melt viscosity [17]. Such behavior is maintained in the VZ-Cs glasses even with the addition of the simulated waste (Cs-loaded zeolite), as VZ8-Cs composition exhibit homogeneous surfaces.

The X-ray diffractometry patterns in Fig. 3 show no crystalline phases, but rather typical amorphous halos for all analyzed wasteform compositions, confirming the glassy state of these specimens.

The network structure of all the glass wasteforms specimens analyzed by Raman (Fig. 4) is predominantly built of SiO_4 tetrahedra (Q^2), interconnected by two bridging-oxygens (BO), each tetrahedra also containing two non-bridging oxygens (NBO). The spectra reveals that all glass wasteform compositions are influenced by the Nb presence. This influence grows with the increase of the Nb content. Also, the deconvolution applied shows other less intense interferences in species Q^1, Q^3, Q^4, boron and aluminates species. As seen from the bands area (%) shown in Table 2, the growth of Nb content promotes changes in the network structure, resulting in the fluctuations of several units such as the overall stretching of SiO_4 tetrahedra (Si–O–Si), Q^1, BO, Q^3 and Q^4, indicating the increase in discontinuities (NBO's). The present cations (Na^+, Ca^{2+}, K^+, Cs^+) are also influenced by the changes in NBO's concentration, as their location depends on each specific valence number. The short-angled Al–O–Al units decrease at the expense of regular Al–O–Al units, in response to network adaptations. Changes in the borate units take place by the decrease in borosilicate rings, increase in tetraborate groups and decrease of BO^3 units. The diborate units increase proportionally to the Nb content, showing adaptations related to the charge balancing cations (Na^+) in the boron-subnetwork. The

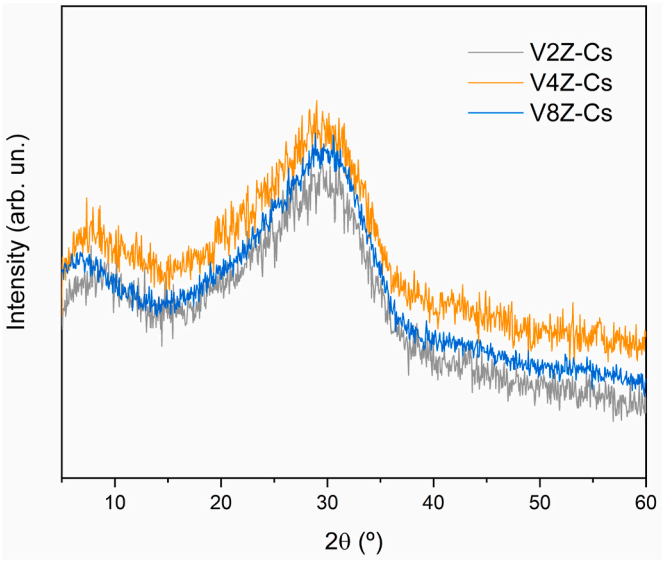

Fig. 3. XRD patterns of the wasteforms containing Cs immobilized in the glassy state.

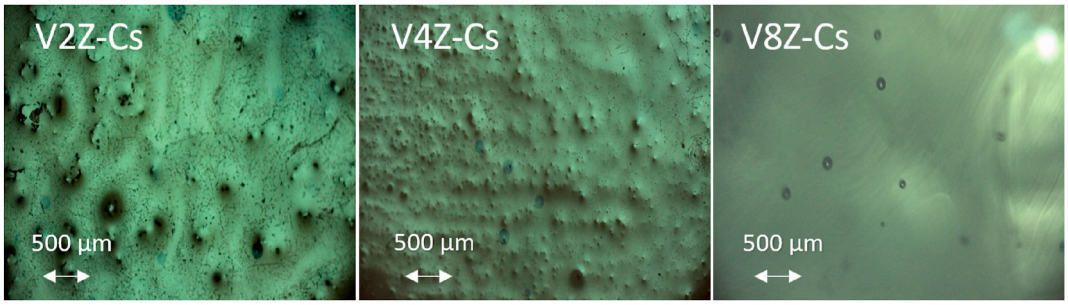

Fig. 2. Transmitted light optical micrographs of the vitreous wasteforms.

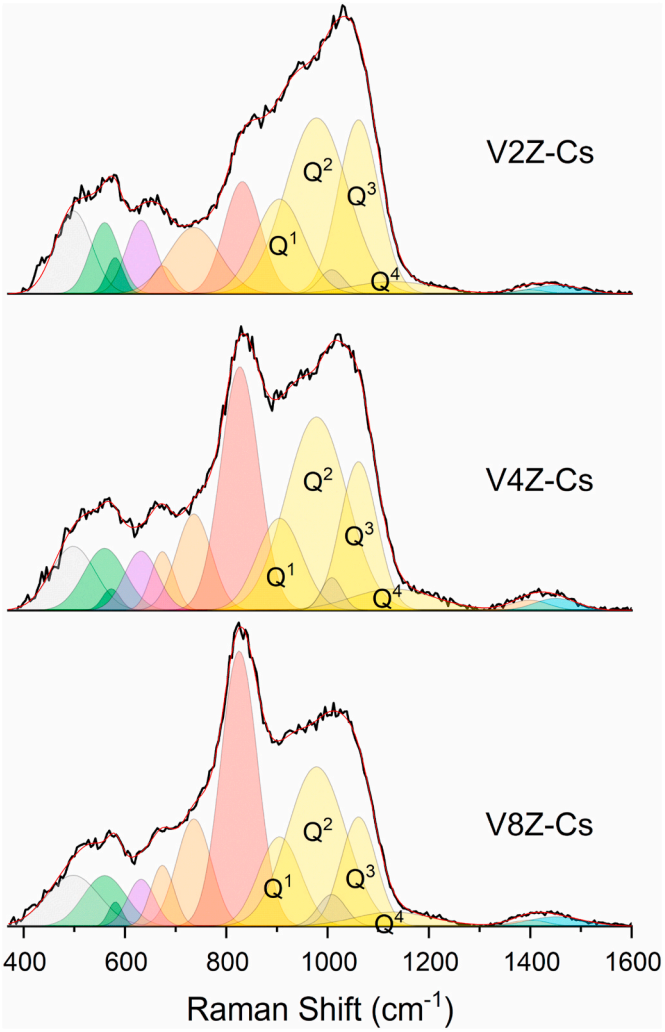

Fig. 4. Room temperature Raman spectra of the glass wasteform samples with deconvoluted bands.

Table 2
Relative area (%) of Raman bands obtained from the deconvolution procedure ($\sigma = 0.073$; R2 = 0.981).

Structural bands stretching	Raman Shift (cm^{-1})	V2Z-Cs	V4Z-Cs	V8Z-Cs
Si–O–Si	498	7.44	5.84	6.01
Al–O–Al	560	5.08	7.04	6.38
Al–O–Al (short-angled)	575	1.57	0.61	0.94
Si–O–B–O–Si borosilicate rings	632	5.35	3.95	3.91
BO_4 tetraborate groups	674	2.64	3.00	3.54
BO_4 diborate groups	736	7.48	8.12	10.67
Nb–O–Nb stretching in NbO_6 units	816	11.73	18.29	22.60
Q^1 units (SiO_4, 1 bridging oxygen)	905	12.06	12.64	9.51
Q^2 units (SiO_4, 2 bridging oxygens)	978	18.66	22.32	20.65
BO bridging oxygen	1008	8.68	1.18	2.02
Q^3 units (SiO_4, 3 bridging oxygens)	1061	12.46	11.30	8.46
Q^4 units (SiO_4, 4 bridging oxygens)	1129	4.21	3.65	3.75
BO_4 III	1398	0.55	0.74	0.52
BO_3	1450	2.09	1.33	1.04

Nb–O–Nb stretching increases substantially due to the increase in Nb content, and to its polarizability for Raman scattering. From V2Z-Cs to V8Z-Cs, there is an increase in Q^2 units, while Q^3 exhibit decrease, Q^1 increases for V4Z-Cs and decreases for V8Z-Cs. Besides, there is a substantial decrease in bridging-oxygen vibrations (BO), but the Q^4 concentrations slightly varies in similarity to BO.

Such variation in the Q^N units with the Nb content, inducing an increase in Q^2, is a new behavior that is opposite from the decrease in these units, which was previously observed for the raw glass matrices, without the Cs-loaded zeolite incorporation [17]. All these changes are rather complex and show that Nb interacts differently in the raw glass matrices than in the wasteforms. This behavior may be explained by the fact that the vitrification projected the glass composition to a system containing more aluminum, and less sodium, calcium and boron. In this case, the growth of Q^2 units at the expense of Q^3, indicates that NbO_6 octahedra interacts with the Q^3 species, however, its role of modifier agent is maintained in both systems, as well as its benefits such as improved homogeneity and melting conditions.

During long-term disposal of glassy wasteforms, temperatures up to 600 °C might be easily reached due to radioactive decay processes [28]. Given the amount of Cs (non-radioactive) immobilized in the VZC-Cs (medium of 5.2 wt% for Cs_2O), dose calculations for ^{137}Cs radionuclide were performed, according to known procedures [29], and the initial activity of 8.1 TBq would imply an accumulated dose of around 0.33 GGy for each 100 g of glass, for the first 12 months. Thus, knowing the thermal behavior of glass matrices for nuclear applications is an important pre-requisite test.

The differential thermal analysis (DTA) performed for our compositions (Fig. 5), shows the endothermic deviation around 520 °C, attributed to the glass transition (T_g), the interval in which the structure starts to lose the glass stiffness. Right away, there is an exothermic deviation from 674 °C to 685 °C that is related to the initial crystallization (T_{ic}). The thermograms show that both temperatures T_g and T_{ic} are slightly influenced by Nb content. However, the Nb influence on the T_c (crystallization temperature) is markedly noticed by the displacement of the peaks in temperatures between 748 and 825 °C. Following the heating path, the newly grown crystals are then melted (T_m), and the fluctuations in melting point are associated to structural characteristics of the compositions, such as the decrease in Si–O–Si and BO for V4Z-Cs. Also, the stability of NbO_6 octahedra plays a role as a barrier for atomic diffusion in temperatures below the melting point, as will be shown in next section regarding thermal treatments. These temperatures compose

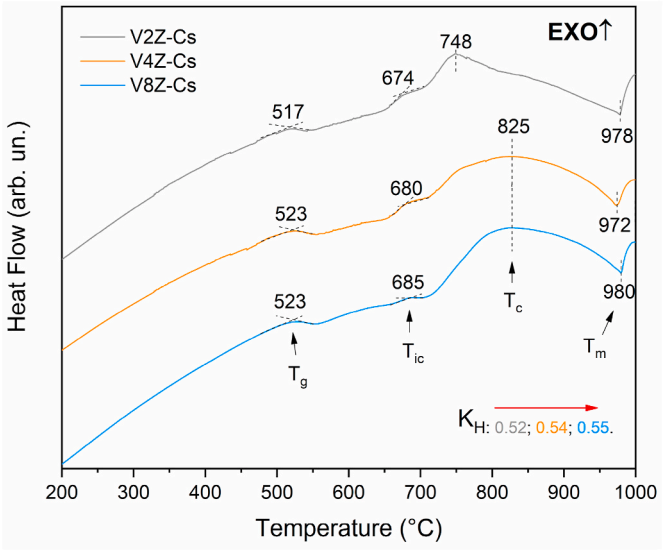

Fig. 5. Differential thermal analysis (DTA) of the glass samples at 10 °C/min up to 1000 °C.

the calculations for the thermal stability by the Hruby parameter (K_H) [24]. The K_H slightly raised from V2Z-Cs to V8Z-Cs, which is another positive influence of the Nb content, and besides that, the three compositions demonstrate a high glass-forming ability ($K_H > 0.5$).

Based on the DTA thermal results, the crystallization behavior of the wasteforms was assessed by heat treatments for 2 h at 520 °C, 685 °C and 800 °C. No crystallization was observed up to 520 °C by the X-ray diffraction patterns (Fig. 6-a). However for specimens heat treated at 685 °C (Fig. 6-b) and 800 °C (Fig. 6-c), the XRD patterns show crystallization of four distinct phases: (1) sodium niobate Lueshite ($NaNbO_3$; CIF nº 5910011), (2) cesium aluminum silicate Pollucite ($Cs_4Al_4Si_2O_6$; CIF nº 9001797), (3) soda-lime silicate Combeite ($Na_2Ca_2Si_3O_9$; CIF nº 9007720) and (4) sodium aluminum silicate Nepheline ($NaAlSiO_4$; CIF nº 9010480). Interestingly, the intensity of the Lueshite phase peaks is higher for samples treated at 800 °C than for 685 °C. Comparing V8Z-Cs in both temperatures, the Lueshite peaks at 22 (2θ), 32 (2θ) and 46 (2θ), whose normalized intensities are respectively 36, 48 and 71 for the sample treated at 685 °C (Fig. 6-b), change respectively 83, 80 and 108, for the sample treated at 800 °C (Fig. 6-c). This fact suggests that Nb is retained in the glassy phase up to 685 °C. The behavior of these glass-ceramics materials has been studied in parallel with this work, with promising results.

An important characteristic of glass classification for use as waste-form is its hydrolytic resistance. After 7 days under the PCT-B tests on the particles under a high surface area/leachate volume, Fig. 7 (a) shows the element release and Fig. 7 (b) the normalized leaching rates. The samples V4Z-Cs and V8Z-Cs exhibited lower leaching rate of Na and Cs, than V2Z-Cs. This fact suggests that the network adaptation for these specific Nb contents, such as the increase of the predominant structural units (Q^2) plays an important role. As these units are composed SiO_4 planes, the increase of percolation channels in the network structure favors the dispersion of the highly distorted NbO_6 octahedra, as already observed in our previous work related to these glasses [17]. On the other hand, such bulky and distorted octahedra might act as barriers and difficult the diffusion of large radius hydrated ions such as Cs^+ and Ca^{2+}. The concentration on the leachates is on average 5 times higher for Na than for Si, Al, Ca, B and Cs, due to the strong interaction of Na^+ ions in water, being the first to be hydrolyzed, and due to the elevated Na content on the glasses. However, in addition to showing similar behavior, the leaching rates (Fig. 7-b) exhibit the decrease and stabilization of Cs leaching from V2Z-Cs to V8Z-Cs at around 1.5×10^{-3} g m^{-2}, meeting the pre-requisites for high-level waste (HLW) immobilization and long-term disposal [30–32].

Despite showing a strong influence in the glassy phase, Nb was not detected on the aliquots by the NAA technique, that is, the element is strongly attached to the network structure, as previously verified by Raman spectroscopy. However, if present in the leachants, its concentration is below the detection limit (3.3 mg/kg), showing its high insolubility in water attack. The initial pH measured in the leachants was 7.0 ± 0.5, and the final pH was 13.0 ± 0.5, measured from the leachates (final solutions resulting from the experiment), at room temperature. Such increase in pH for the leachates can be explained by the higher elemental release of Na^+, when compared to the other analyzed elements (Cs, Si, Ca, Al and B). In the initial state of PCT-B tests (neutral pH), water interacts with the alkali ions located near the NBO's to produce hydroxyl groups (OH^-), which increases the pH and releases the alkali ions into the solution [33]. Therefore, the leaching behavior of the glass wasteform samples (Fig. 7 a and b) is influenced by the contact time, the saturation of elements and the basic pH of the leachates, leading the hydrolysis to achieve a steady state. The rates for all analyzed elements are in the range that is currently acceptable for application as nuclear glasses ($\leq 10^{-3}$ g m^{-2}) [30,31], turning these compositions into safe options for immobilizing radioactive Cs. The impact of Nb in the leaching rates is subtle, and more expressive for Na and Cs than for the other elements. The V8ZCs composition, due to its strong Nb contribution, reveals to be a potential candidate for use in the

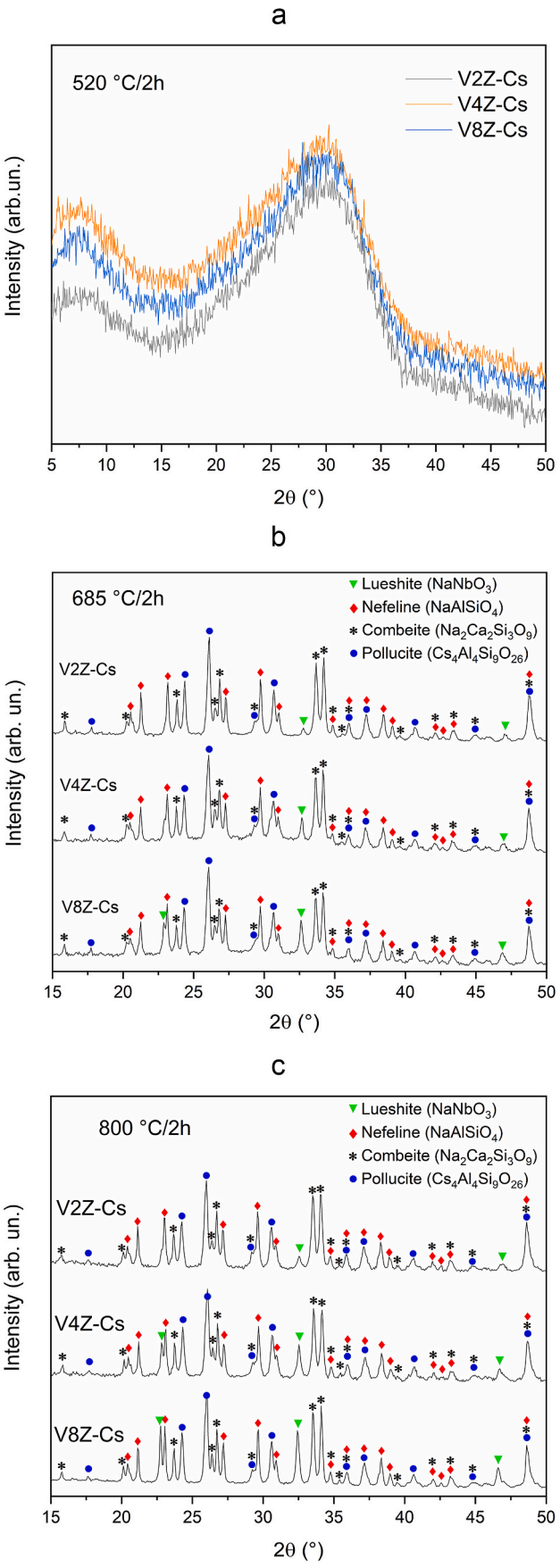

Fig. 6. X-ray diffraction patterns of the glass samples after the heat treatments: (a) at 520 °C, (b) at 685 °C and (c) at 800 °C.

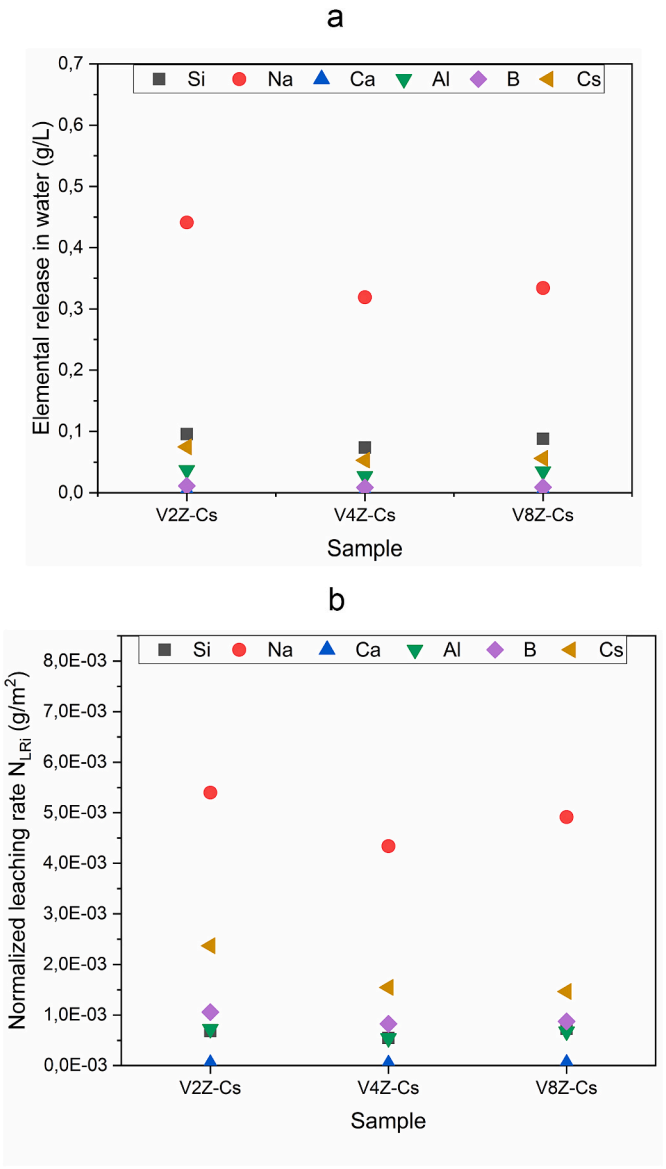

Fig. 7. Elemental release in water (a) and normalized leaching rate of elements (b) on the aliquots after the PCT-B leaching for 7 days.

immobilization of the ^{137}Cs adsorbed by zeolitic structures, due to its good results in uniform structure, thermal stability, and mainly hydrolytic resistance.

4. Conclusions

The vitrification of a Cs-loaded zeolite waste was explored in aluminoborosilicate glass matrices optimized with Nb, and the atomic structure could be analyzed and associated with thermal and leaching properties. The melt homogeneity of the produced wasteforms was found to be improved with 8.0 mol% Nb. The Cs-loaded zeolite was completely incorporated in the glassy phase, adding up to 5.9 wt% of Cs_2O to the global compositions and 18% SiO_2, 11.8% Al_2O_3 along with minor impurities from the zeolitic material, corresponding to a 53% efficiency (Cs immobilization). Nb contents influenced the network structure by the growth of predominant Q^2 species at the expense of Q^3, with rearrangements in Q^1, Q^4, borate and aluminate units, reflecting on thermal and leaching properties. The glass wasteforms' structure is composed of a wide Q^2 open framework, containing a partial content of boron and aluminum acting as glass formers, and several discontinuities (NBO's) that are charge balanced by the present cations, including Cs. The three compositions showed adequate thermal glass stability for nuclear applications ($K_H > 0.5$), and were stable up to 520 °C, crystallizing at 685 °C, with full consolidation at 800 °C for the niobium phase, leading to four crystalline phases: Lueshite ($NaNbO_3$), nepheline ($NaAlSiO_4$), Combeite ($Na_2Ca_2Si_3O_9$) and Pollucite ($Cs_4Al_4Si_9O_{26}$). The chemical resistance of the glassy wasteforms after leaching at 90 °C for 7 days in static conditions exhibited low leaching rates for Cs, meeting the pre-requisites for nuclear glasses ($\leq 10^{-3}$ g m^{-2}). The most adequate composition among the three was V8Z-Cs (8.0 mol% Nb), due to its notable thermal stability and high hydrolytic resistance, promising characteristics for the immobilization of ^{137}Cs.

Declaration of competing interest

The authors declare that they have no known competing financial interests or personal relationships that could have appeared to influence the work reported in this paper.

Acknowledgments

The authors would like to thank Instituto de Pesquisas Energéticas e Nucleares (IPEN/USP) for the lab facilities and the financial support from project 2020.06.IPEN.27.

References

[1] Emara AM, Elsharma EM, Abdelmonem IM. Adsorption of radioactive cesium using synthesized chitosan-g-poly(acrylic acid/N-vinylcaprolactam) by γ-irradiation. Radiat Phys Chem 2023;208. https://doi.org/10.1016/j.radphyschem.2023.110892.
[2] Abbas TK, Rashid KT, Alsalhy QF. NaY zeolite-polyethersulfone-modified membranes for the removal of cesium-137 from liquid radioactive waste. Chem Eng Res Des 2022;179. https://doi.org/10.1016/j.cherd.2022.02.001.
[3] Caruso S, Meleshyn A, Noseck U. Estimation and comparison of the radionuclide inventories in vitrified high-level wastes from reprocessing plant. Prog Nucl Energy 2017;94. https://doi.org/10.1016/j.pnucene.2015.11.003.
[4] Sopapan P, Lamdab U, Akharawutchayanon T, Issarapanacheewin S, Yubonmhat K, Silpradit W, Katekaew W, Prasertchiewchan N. Effective removal of non-radioactive and radioactive cesium from wastewater generated by washing treatment of contaminated steel ash. Nucl Eng Technol 2023;55. https://doi.org/10.1016/j.net.2022.10.007.
[5] Yasunari TJ, Stohl A, Hayano RS, Burkhart JF, Eckhardt S, Yasunari T. Cesium-137 deposition and contamination of Japanese soils due to the Fukushima nuclear accident. Proc Natl Acad Sci USA 2011;108:19530–4. https://doi.org/10.1073/pnas.1112058108.
[6] Jiménez-Reyes M, Almazán-Sánchez PT, Solache-Ríos M. Radioactive waste treatments by using zeolites. A short review. J Environ Radioact 2021;233:106610. https://doi.org/10.1016/j.jenvrad.2021.106610.
[7] Mahima Kumar M, Irshad KA, Jena H. Removal of Cs+ and Sr2+ ions from simulated radioactive waste solutions using Zeolite-A synthesized from kaolin and their structural stability at high pressures. Microporous Mesoporous Mater 2021;312:110773. https://doi.org/10.1016/j.micromeso.2020.110773.
[8] Muslim WA, Albayati TM, Al-Nasri SK. Decontamination of actual radioactive wastewater containing 137Cs using bentonite as a natural adsorbent: equilibrium, kinetics, and thermodynamic studies. Sci Rep 2022;12. https://doi.org/10.1038/s41598-022-18202-y.
[9] Voronina AV, Noskova AY, Semenishchev VS, Gupta DK. Decontamination of seawater from 137Cs and 90Sr radionuclides using inorganic sorbents. J Environ Radioact 2020;217. https://doi.org/10.1016/j.jenvrad.2020.106210.
[10] Lee K, Kim J. Immobilization of 137Cs as a crystalline pollucite surrounded by amorphous aluminosilicate. Environ Res 2023;221. https://doi.org/10.1016/j.envres.2023.115309.
[11] Kuenzel C, Cisneros JF, Neville TP, Vandeperre LJ, Simons SJR, Bensted J, Cheeseman CR. Encapsulation of Cs/Sr contaminated clinoptilolite in geopolymers produced from metakaolin. J Nucl Mater 2015;466:94–9. https://doi.org/10.1016/j.jnucmat.2015.07.034.
[12] Kimura R, Inagaki Y, Idemitsu K, Arima T. Vitrification processes of simulated cesium sorbing zeolite waste. Prog Nucl Energy 2018;108. https://doi.org/10.1016/j.pnucene.2018.01.001.
[13] Fu J, Zhao J, Li S, Zhang H, Shi S, Zhang J, Liu S. Influence of CeO2 on the structure and properties of borosilicate glass: an investigation from the perspective besides the refining process. J Non-Cryst Solids 2024;623:122690. https://doi.org/10.1016/j.jnoncrysol.2023.122690.
[14] Sheng J, Choi K, Song MJ. Vitrification of liquid waste from nuclear power plants. J Nucl Mater 2001;297. https://doi.org/10.1016/S0022-3115(01)00598-0.

[15] Sobolev IA, Dmitriev SA, Lifanov FA, Kobelev AP, Stefanovsky SV, Ojovan MI. Vitrification processes for low, intermediate radioactive and mixed wastes, vol 46. Glass Technology; 2005. p. 28–35.
[16] Vernaz E, Veyer C, Gin S. Waste glasses, comprehensive nuclear materials. second ed. 2016. p. 414–44. https://doi.org/10.1016/B978-0-12-803581-8.00758-X.
[17] Costa-silva DL, Bartolomé JF, Silva AC, Mello-Castanho S. Structural and thermal influence of niobia in aluminoborosilicate glasses. Ceram Int 2022;48:18433–40. https://doi.org/10.1016/j.ceramint.2022.03.112.
[18] Izidoro J, Castanho D, Rossati C, Fungaro D, Guilhen S, Nogueira T, De Fátima Andrade M. Application of high-purity zeolite a synthesized from different coal combustion by-products in carbon dioxide capture. Int J Environ Impacts: Management, Mitigation and Recovery 2019;2:215–28. https://doi.org/10.2495/EI-V2-N3-215-228.
[19] Tian Q, Sasaki K. Application of fly ash-based materials for stabilization/solidification of cesium and strontium. Environ Sci Pollut Control Ser 2019;26:23542–54. https://doi.org/10.1007/s11356-019-05612-1.
[20] Wojdyr M. Fityk: a general-purpose peak fitting program. J Appl Crystallogr 2010;43. https://doi.org/10.1107/S0021889810030499.
[21] Manara D, Grandjean A, Neuville D. Advances in understanding the structure of borosilicate glasses: a Raman spectroscopy study. Am Mineral 2009;94:777–84. https://doi.org/10.2138/am.2009.3027.
[22] Lönartz MI, Dohmen L, Lenting C, Trautmann C, Lang M, Geisler T. The effect of heavy ion irradiation on the forward dissolution rate of borosilicate glasses studied in situ and real time by fluid-cell Raman spectroscopy. Materials 2019;12:1480. https://doi.org/10.3390/ma12091480.
[23] De Andrade JS, Pinheiro AG, Vasconcelos IF, De Araújo MAB, Valente MA, Sombra ASB. Structural studies of KNbO3 in niobate glass-ceramics. J Phys Chem Solid 2000;61. https://doi.org/10.1016/S0022-3697(99)00387-X.
[24] Kozmidis-Petrovic A, Šesták J. Forty years of the Hrubý glass-forming coefficient via DTA when comparing other criteria in relation to the glass stability and vitrification ability. In: J therm anal calorim; 2012. https://doi.org/10.1007/s10973-011-1926-6.
[25] Yokomori Y, Asazuki K, Kamiya N, Yano Y, Akamatsu K, Toda T, Aruga A, Kaneo Y, Matsuoka S, Nishi K, Matsumoto S. Final storage of radioactive cesium by pollucite hydrothermal synthesis. Sci Rep 2014;4:4195. https://doi.org/10.1038/srep04195.
[26] Wang J, Zhuang S. Removal of cesium ions from aqueous solutions using various separation technologies. Rev Environ Sci Biotechnol 2019;18. https://doi.org/10.1007/s11157-019-09499-9.
[27] Jain S, Banthia N, Troczynski T. Leaching of immobilized cesium from NaOH-activated fly ash-based geopolymers. Cem Concr Compos 2022;133:104679. https://doi.org/10.1016/j.cemconcomp.2022.104679.
[28] Lago DC, Sánchez AD, Prado MO. Immobilization of a simulated high-level waste in an yttrium aluminosilicate glass. Self-heating assessment. J Eur Ceram Soc 2022;42. https://doi.org/10.1016/j.jeurceramsoc.2022.08.048.
[29] Turner JE. Atoms, radiation, and radiation protection. Third Edition; 2007. https://doi.org/10.1002/9783527616978.
[30] Ojovan MI, Lee WE, Kalmykov SN. Chapter 19 - immobilisation of radioactive wastes in glass. In: Ojovan MI, Lee WE, Kalmykov SN, editors. An introduction to nuclear waste immobilisation. third ed. Elsevier; 2019. p. 319–68. https://doi.org/10.1016/B978-0-08-102702-8.00019-4.
[31] Ojovan MI, Petrov VA, Yudintsev SV. Glass crystalline materials as advanced nuclear wasteforms. Sustainability 2021;13. https://doi.org/10.3390/su13084117.
[32] Chen T-Y, Maddrell ER, Hyatt NC, Hriljac JA. A potential wasteform for Cs immobilization: synthesis, structure determination, and aqueous durability of $Cs_2TiNb_6O_{18}$. Inorg Chem 2016;55:12686–95. https://doi.org/10.1021/acs.inorgchem.6b01826.
[33] Gan XY, Zhang ZT, Yuan WY, Wang L, Bai Y, Ma H. Long-term product consistency test of simulated 90-19/Nd HLW glass. J Nucl Mater 2011;408. https://doi.org/10.1016/j.jnucmat.2010.11.020.